Substorm Activity as a Driver of Energetic Pulsating Aurora

R. N. Troyer [1], A. N. Jaynes [1], S. L. Jones [2], S. R. Kaeppler [3], R. H. Varney [4], A. S. Reimer [5]

[1]Department of Physics and Astronomy, University of Iowa
[2]Formerly of NASA Goddard Space Flight Center
[3]Clemson University
[4]Department of Atmospheric and Oceanic Sciences, University of California, Los Angeles
[5]Formerly of SRI International

Key Points:

- We analyzed the inverted energy content for 53 pulsating aurora events and found a close relationship to substorm onset and AE index.
- The average total energy flux and hardness increase closer to substorm onset and for higher AE indices.
- The energy hardness remains enhanced for approximately 1 hour after substorm onset.

Corresponding author: Riley Troyer, `riley-troyer@uiowa.edu`

Abstract

Pulsating aurora are common diffuse-like aurora. Studies have suggested that they contain higher energy particles than other types and are possibly linked to substorm activity. There has yet to be a quantitative statistical study of pulsating aurora energy content. We analyzed the inverted energy content from 53 events using the Poker Flat Incoherent Scatter Radar. We compared this to magnetic local time (MLT), AE index, and temporal proximity to substorm onset. There was a slight trend in MLT, but a much stronger one in relation to both substorm onset and AE index. For higher AE and closer to onset the total energy flux and flux above 30 keV increased. In addition, this higher energy remained enhanced for an hour after substorm onset. Our results confirm the high energy nature of pulsating aurora, demonstrate the connection to substorms, and imply their importance to coupling between the magnetosphere and atmosphere.

Plain Language Summary

Not all aurora (northern lights) are bright and defined curtains of light. Diffuse aurora are more modest. Barely visible to the naked eye, they spread across large portions of the night sky and can be easily overlooked. Pulsating aurora are a common and more playful type of diffuse aurora. In one of these displays, widely varying patches of aurora blink on and off with with periods ranging up to 20 seconds. While they aren't as bright, it has been suspected that the electrons which cause pulsating aurora are much more energetic than other types of aurora. Since energetic electrons move faster and thus can reach further into the atmosphere, it is possible that pulsating aurora may affect terrestrial climate. To study this, we first need a better understanding of pulsating aurora energies and how they can vary. In this study, we looked at the energy of 53 pulsating aurora events. In doing so, we confirmed that the energy of pulsating aurora is much higher than other types of aurora. We also found that the most energetic aurora happen close in time to a magnetic disturbance known as a substorm and that a stronger disturbance leads to higher energies.

1 Introduction

Pulsating aurora are a stark contrast to the bright curtains of discrete aurora that often precede them. Diffuse and barely visible to the naked eye, this type of aurora is

most often observed a few hours after magnetic midnight (e.g., Oguti et al., 1981; Jones et al., 2011). Often staying out for hours, pulsating aurora can cover large portions of the sky and in some cases expand over entire sections of the auroral region (Jones et al., 2013). Using SuperDarn and imager data, E. Bland et al. (2021) found that around half of pulsating aurora events extend between 4-5 hours of magnetic local time and between 62° to 70° in magnetic latitude. Over this area, auroral patches blink on and off with periods ranging up to around 20 seconds (e.g., Davis, 1978; Lessard, 2012). Adding to the auroral display, individual patches can be remarkably varied with differing periods, shapes, and sizes typically between 10s to 100s of kilometers (Johnstone, 1978; Lessard, 2012). Figure 1 panels A1-A3 shows a typical example of pulsating aurora that occurred on October 13, 2016 over the Poker Flat Research Range. The red oval highlights a patch that turns on and off during the three images.

Numerous studies have shown that the electrons responsible for pulsating aurora originate in the equatorial region of the outer Van Allen radiation belt. These electrons are pitch-angle scattered into the upper-atmosphere through wave-particle interactions, most likely with lower-band chorus waves (Nishimura et al., 2010, 2011; Jaynes et al., 2013; Kasahara et al., 2018; Hosokawa et al., 2020). Previous studies have found that the energy range of pulsating aurora electrons is substantially higher than other auroral types, ranging between 10s to 100s of keV (e.g., Whalen et al., 1971; Sandahl et al., 1980). Both the total energy flux and hardness can vary, even within individual events. Jones et al. (2009) notes often seeing a decrease in the differential energy flux of 0.5 to 32.5 keV electrons throughout an event. Hosokawa and Ogawa (2015) found, using the European Incoherent Scatter Radar, that the energy spectrum of pulsating aurora is harder when a patch is "on" versus when it is "off" with only background aurora present.

Some studies have attempted to classify different types of pulsating aurora. For instance, Royrvik and Davis (1977) classified events into patches, arcs, and arc segments. More recently, Grono and Donovan (2018) made a distinction between the quickly varying amorphous pulsating aurora (APA), more regular patchy pulsating (PPA) aurora, and non-pulsating patchy aurora (nPPA). Tesema et al. (2020) used incoherent scatter radar to look at the electron density profile between APA, PPA, and nPPA. They found that PPA and nPPA were associated with enhanced electron densities below 100 km when compared with APA.

Several papers regarding the the height of pulsating aurora indicate that there may be a relation between peak differential energy flux of precipitating electrons and substorm onset. In the two events that Oyama et al. (2017) analyzed, they found a drop to lower altitudes following substorm onset in the atmospheric electron densities of pulsating aurora. This would indicate an influx of higher energy electrons capable of penetrating further into the atmosphere. These results are similar to the statistical study of Hosokawa and Ogawa (2015) who showed that the electron density profile of pulsating aurora extends lower in altitude during periods with a large AE index (> 500). This previous work is a strong indicator of the increase in higher energy electrons, or hardening, during geomagnetic activity that causes an increase in AE index. However, the results are qualitative as altitude is only a proxy for energy. Wing et al. (2013) did conduct a statistical study of auroral energies associated with substorm onset. They made distinctions between broadband (Alfvén accelerated) electrons, monoenergetic (parallel electric field accelerated) electrons, and diffuse (whistler mode wave scattered) electrons. They found that total energy flux increases in association to substorm onset for all types, with the largest for diffuse electrons. However, they made no distinction between general diffuse and pulsating aurora.

These previous investigations make a strong case for a link between substorm onset and AE index and both the total energy flux and spectral hardness of pulsating aurora. More energetic events seem to occur right after substorm onset and for higher AE indices. However, direct evidence supporting this hypothesis has yet to be established. Providing this evidence will be an important step in understanding how energy is transferred from the magnetosphere to the atmosphere. There are many reasons why this is important, but one which has recently become more apparent is the depletion of ozone due to pulsating aurora produced NO_x (Turunen et al., 2016; Verronen et al., 2021). In this paper, we provide statistical evidence, using inverted differential energy fluxes, that substorm onset and AE index are indeed correlated with a higher differential energy flux and a harder energy content in pulsating aurora. The results shown here both confirm the high-energy nature of pulsating aurora and specify how pulsating aurora energies are correlated with substorm onset and AE index.

2 Data

This paper presents a data set of 57 pulsating aurora events between 2012 and 2021, four of which (2015-01-13, 2017-08-17, 2018-12-30, and 2021-01-13) were not usable for our energy inversion. We visually identified pulsating aurora using all sky images and used the classifications of both (Royrvik & Davis, 1977) and (Grono & Donovan, 2018) when doing so. This data was captured over 51 days with the Poker Flat Research Range All Sky Imager (PFRR ASI). A table with the dates of all 51 days can be found in the supplemental material. This instrument takes an image approximately every 12 seconds at 428 nm, 557 nm, and 630 nm. We used the 428 nm images. It is worth noting that despite the 12 second period of the camera, we can still accurately identify pulsating aurora, see Figure 1 panels A1-A3 as an example.

For each of these pulsating aurora events, the Poker Flat Incoherent Scatter Radar (PFISR) was running one of the D-region modes (MSWinds23, MSWinds26, or MSWinds27). For more details about these modes than we describe here, see Kaeppler et al. (2020). These modes all use 13-baud Barker codes with 10 μs baud, oversampled at 5μs (0.75 km range resolution) to provide electron density as function of range and time over ranges between 40 to 144 km. This study uses one minute integration times, which means the electron density profiles are averaged over many cycles of the pulsating aurora. These modes all use four beam directions (magnetic zenith, vertical, north-west, and north-east). This study uses the vertical beam data since it is systematically more sensitive than the magnetic zenith direction at PFISR. The magnetic zenith is close to the phased-array antenna grating lobe steering limit. Furthermore, the MSWinds27 modes revisit the beams unevenly such that the vertical beam receives 16 times more pulses than the other beam directions, resulting in a factor of 4 improvement in the statistical uncertainty relative to the other beam directions. The vertical beam is $< 20^\circ$ away from the magnetic zenith direction which is sufficiently small for our inversions to neglect any variations across magnetic field lines. Supplementary Appendix 2 gives additional information on the PFISR experiments and data processing. Figure 1 panel B shows an example of electron densities measured by PFISR MSWinds23 during a period of typical pulsating aurora on October 13, 2016. This event began less than 15 minutes after a substorm onset and continued until the end of the PFISR experiment.

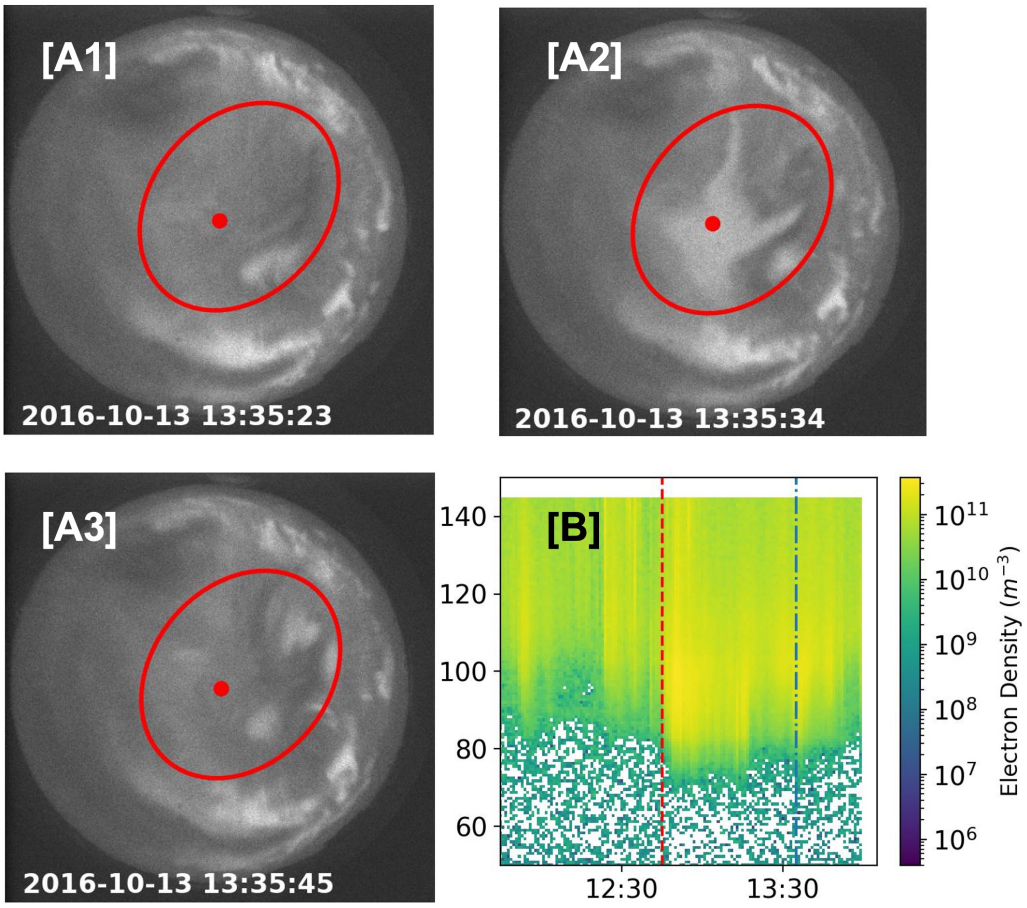

Figure 1. Panels A1-A3 show a series of 428 nm images from the Poker Flat Research Range All Sky Imager with several pulsating aurora patches of differing sizes. Even though the imaging rate is 12 seconds, we can still identify pulsating aurora. The red dot indicates the center of each image and thus the approximate location of the vertical PFISR beam. Panel B is the PFISR electron number density data for a pulsating aurora event on October 13, 2016. The data is plotted vs. altitude in km and universal time. The dashed red line indicates the start of pulsating aurora. The dashed and dotted blue line indicates when the images were taken. The radar stopped taking data before the pulsating aurora ended.

3 Analysis

In this study, we quantify the differential energy flux of pulsating aurora, in particular, the higher energy portion. Previous investigations have indicated that the energy of pulsating aurora varies significantly both within and between events, often associated with substorm activity (Jones et al., 2009; Wing et al., 2013; Hosokawa & Ogawa, 2015). Based on these results, we chose to examine variations related to magnetic local time (MLT), AE index, and an epoch associated with temporal substorm proximity. We set an epoch time of 0 to substorm onsets taken from lists created by Newell and Gjerloev (2011), Forsyth et al. (2015), and Ohtani and Gjerloev (2020). We chose these three lists because they cover a time period that covers the range of dates in our data. Each method identifies substorms in a slightly different way, so by including all three we can identify more events over a broader range of criteria. We limited these substorms to those that occurred within $\pm 15^\circ$ longitude and $\pm 8^\circ$ latitude of the Poker Flat Research Range. For the AE indices, we used archived 10-minute averaged predicted values (Luo et al., 2013). For every 1-minute electron density profile we find the closest in time AE index and assign that to the data point.

As a proxy for energy, we chose the lower altitude boundary that PFISR measured a number density of $N_e = 10^{10}\,\mathrm{m}^{-3}$ for each 1-minute integrated altitude profile. Additionally, to meet this criteria, the associated error had to be less than $5 \times 10^9\,\mathrm{m}^{-3}$. We chose these values somewhat arbitrarily given that they are round numbers near the detection limit of PFISR. However, we did test the sensitivity and found them to be acceptably insensitive. Future, more sensitive instruments could use a smaller density threshold and thus detect lower altitudes. Finally, we implemented an outlier-rejection algorithm to remove high power returns that are not consistent with the expected electron density profile from precipitation. The D-region data can be cluttered by range-aliased satellite echoes, airplanes in antenna sidelobes, and various types of interference. Most of these clutter sources appear as localized outliers in the power data confined to one or two range-gates. We expect a realistic electron density profile to extend over 10s of km in altitude and be monotonically decreasing with altitude. We compute the median electron density over 5 km around a data point and check that it is less than the median electron density 20 km above that point. Furthermore, we check if there are any NaN or negative electron density estimates in the 20 km above that point.

It is more typical for studies to concentrate on the altitude of the peak electron density. We chose a different metric as we wanted a proxy that would more closely represent the flux of higher energy particles. This approach isn't perfect as a higher flux of slightly lower energy particles could produce a similar boundary to a lower flux of higher energy particles. Any altitude metric is still only a proxy for energy, but this one also contains other useful information. One of the main goals of this work is to provide data to help understand the atmospheric effects of pulsating aurora such as ozone depletion. In this regard, atmospheric changes are more important than the original energy flux. Thus, by choosing to measure altitude from a lower boundary instead of the peak electron density, we are able to more closely connect our measurements to possible atmospheric effects.

3.1 Magnetic Local Time

Figure 2 panel A shows the altitude boundary values compared to MLT as calculated from the IGRF model for 2020. As we would expect, a majority of the measurements occurred several hours after magnetic midnight. Previous studies have shown that this is the most common time for pulsating aurora (Oguti et al., 1981; Jones et al., 2011). The hourly averages shown by the black diamonds centered on each hour indicate that there is little, if any, dependence on MLT. Interestingly, previous results have shown a small correlation between peak electron density altitude and MLT (Hosokawa & Ogawa, 2015; Partamies et al., 2017; E. C. Bland et al., 2019; Tesema et al., 2020; Nanjo et al., 2021). It's possible that our data is obscuring this trend due to the wide scatter of data and limited statistics for several time bins. In addition, we requested instrument runs during the most common time for pulsating aurora, so the data is biased towards that period.

3.2 Substorm Onset and AE index

Figure 2 panel B shows the altitude boundary with $N_e = 10^{10}\,\mathrm{m}^{-3}$ compared to substorm onset. Here we see that lower altitudes are more common closer to substorm onset, indicating a hardening of the energy content. These results are similar to that of Oyama et al. (2017), who found both an enhancement and lowering of electron densities just after substorm onsets for several case study pulsating aurora events. Our work extends these findings to a statistical dataset.

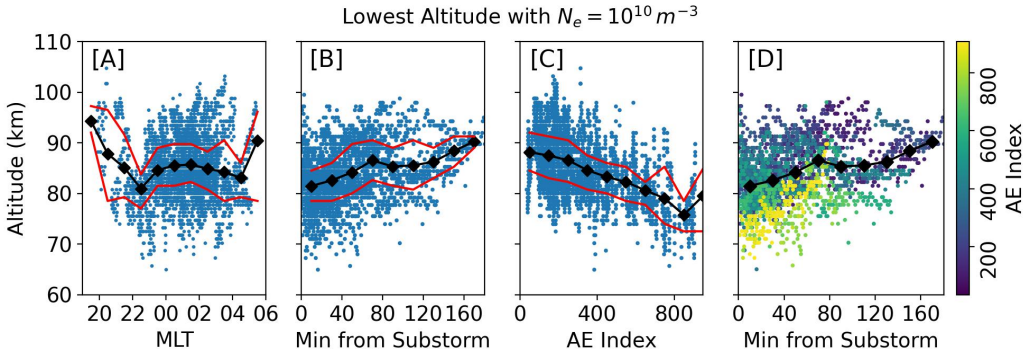

Figure 2. Lowest altitude PFISR measurements during pulsating aurora with $N_e = 10^{10}\,\mathrm{m}^{-3}$ plotted versus magnetic local time [A], time from the nearest substorm onset [B], AE index [C], and combined substorm and AE [D]. The black diamonds indicate the average altitude for the surrounding hour, 20 minutes, 200 AE units, and 20 minutes respectively. The red lines indicate the 25% and 75% quartiles.

Figure 2 panel C shows the altitude boundary with $N_e = 10^{10}\,\mathrm{m}^{-3}$ compared to the closest in time 10-minute averaged AE index. Similar to substorm proximity, there is a clear relation between a higher AE value and lower altitudes. This is similar to the results of Hosokawa and Ogawa (2015) who found that the peak altitude of pulsating aurora lowers during higher AE indices. However, our measurements differ in that the peak altitude is a proxy for an average energy flux, whereas our lower altitude boundary is more representative of the energy content hardness.

We combined Figures 2B and 2C to produce Figure 2 panel D. Here we have colored the markers of Figure 2B based on AE index. This result shows that both temporal substorm proximity and AE index play a role in varying the lower altitude boundary. The lowest altitudes tend to occur with both a high AE index and close temporal proximity to a substorm. In regards to the statistics, our events cover a wide range of AE indices with 10 occurring during periods with AE $>$ 600 and of those 3 with AE $>$ 800.

We also performed a similar analysis using AL indices, but the results did not differ in any meaningful way. A more negative AL index corresponded to lower altitudes. This plot can be found in the supplementary materials.

3.3 Energy Spectra from Electron Density Inversion

Our analysis of the lower altitude boundary with $N_e = 10^{10}\,\mathrm{m}^{-3}$ indicates that both AE index and substorm onset have significant impacts on how hard the pulsating aurora energy content can be. However, this metric is only a proxy for hardness. To investigate further, we solved the inverted problem required to convert the PFISR electron densities into a differential energy flux. To do this, we used the process outlined in Semeter and Kamalabadi (2005). In doing so, we assumed that the pitch angle distribution was isotropic (Whalen et al., 1971; Sandahl et al., 1980), and that the electron density varies slowly compared to the 1-minute PFISR integration time scales. We describe our exact implementation of the inversion process in supplementary Appendix 1. In an analysis like this, there are multiple spectra that could result in a reasonably good fit of the density profile, making the problem ill-defined. To help mitigate this, we chose the solution that maximized the Berg Entropy. As Semeter and Kamalabadi (2005) states, this solution "may be viewed as the most noncommittal approach with respect to the unavailable information." Because of these uncertainties that are inherent to the inversion process, it is not useful to look at the finer shape of the differential energy flux. Instead, to provide a more robust analysis, we chose an energy threshold of 30 keV to separate the low and high portions of the differential energy flux and integrated the two regions. This gives us an average low and high energy flux and limits the dependency of our results on the smaller scale details.

The largest source of error in the inversion process is likely the assumed atmospheric chemistry that connects PFISR observations to an ionization rate. This is still an ongoing area of research, especially for the D-region. As our primary chemistry model we used the Glukhov-Pasko-Inan (GPI) model (Glukhov et al., 1992; Lehtinen & Inan, 2007). This has been shown to perform well for the D-region (Marshall et al., 2019). For the E-region, we set the values above 90 km to those calculated by Gledhill (1986) for nighttime aurora. The Gledhill model is suitably close that of Vickrey et al. (1982) above 90 km and the Vickrey model has been shown to perform well in this region (Sivadas et al., 2017). While we could have used the Vickrey model, we believe the Gledhill model is more relevant for this data. However, both models are only rough estimates. We refer to this adjusted model as GPI+. To provide context to our results calculated using GPI+, we inverted each density profile using three additional chemistry models. These results, along with other possible sources of errors, can be found in the supplementary Appendix.

After performing the inversions, we found the geometric mean for ≥ 30 keV and < 30 keV electrons in bins relative to substorm onset and AE index. Figure 3 shows the results and demonstrates the link between energy and substorm activity. This figure shows how the energy composition of pulsating aurora varies with respect to both substorm proximity [A] and AE index [B]. Within an hour of a substorm around a third of the total differential energy flux is carried by ≥ 30 keV electrons. At > 60 minutes this drops to around a sixth. Interestingly, while the total differential energy flux climbs closer to the substorm, the energy composition remains similar all the way out to an hour after onset. This indicates that the initial substorm "kick" hardens the energy content and it remains hard up to an hour afterwards, even as the total differential energy flux decreases.

The differential energy flux associated with AE index varies even more dramatically. In highly perturbed times of AE > 600 over a half of the average differential energy flux is carried by the ≥ 30 keV electrons. This again drops to just over a tenth for quiet periods of AE ≤ 200. We also looked at the differential energy flux relative to AL indices, but found no difference to AE beyond a few percent.

Assumptions about the atmospheric chemistry can vary the absolute differential energy flux, but for every model we found the same relative behavior. While not shown here, the relative behavior was also the same when we used threshold values of 50 keV and 100 keV. For < 20 min the high energy contributions were 13.9% and 1.2% respectively. For > 600 AE these were 37.8% and 2.4% respectively. Thus, we speculate with a high level of confidence that pulsating auroral energy content is varied by both the strength of a substorm as well as temporal proximity to it.

4 Discussion

Our work builds on the likes of Wing et al. (2013), Hosokawa and Ogawa (2015), and Oyama et al. (2017), whose studies showed that the altitude of pulsating aurora can lower after substorm onset and for periods of high AE index. It also builds on papers such as Jones et al. (2009), which demonstrated that the inverted differential energy flux of particular pulsating aurora events can vary throughout the event duration. This past work provides evidence that the total energy flux and spectral hardness of pulsating au-

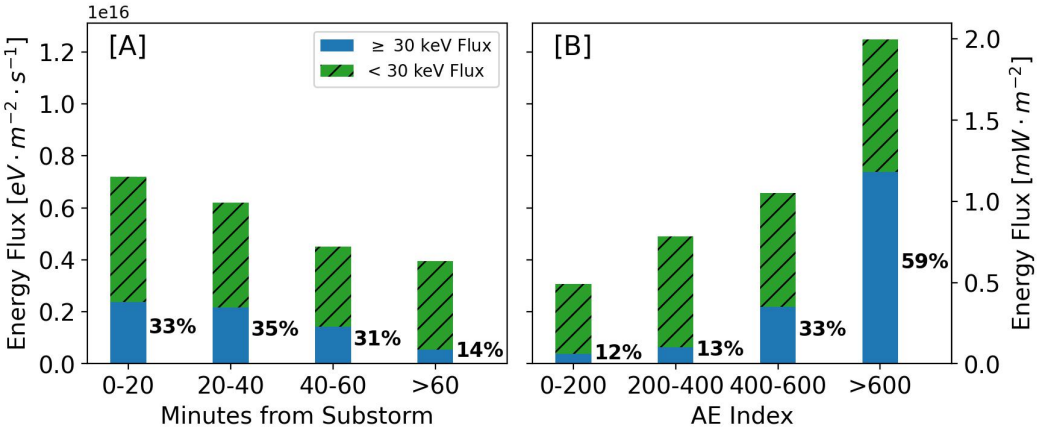

Figure 3. The high ($\geq$ 30 keV) and low ($<$ 30 keV) differential energy flux contributions to pulsating aurora events occurring in four temporal bins relative to substorm onset [A] and AE index [B].

rora could be influenced by substorm onset and AE index, but does not make a direct statistical connection.

The results shown in Figure 3 are significant as they provide a statistical connection in several ways. First, they show that the total differential energy flux of pulsating aurora is highly variable. Second, they show that pulsating aurora events can have large, and in some cases majority, contributions from $\geq$ 30 keV electrons, which represents a hard energy content relative to other auroral types. Third, they show that these quantities are strongly correlated with substorm onset and AE index. These statistical links have never been demonstrated before with inverted differential energy flux and they suggest a process connecting substorms and pulsating aurora.

The link between substorms and pulsating aurora is likely through whistler-mode waves, which are known to drive instances of pulsating aurora (Nishimura et al., 2010, 2011; Jaynes et al., 2013; Kasahara et al., 2018; Hosokawa et al., 2020). There is a well documented relation between substorm activity post-midnight and whistler-mode wave generation near the equator (Tsurutani & Smith, 1974; Thorne et al., 1974). The proposed mechanism connecting them is Doppler-shifted cyclotron resonance with 10-100 keV substorm injected electrons (Dungey, 1963; Kennel & Petschek, 1966). In addition, the amplitude of already present whistler-mode waves can vary with substorm injection. Meredith et al. (2000) showed that between 3.8 $< L <$ 6 whistler-mode amplitudes

increased after a substorm and then decayed with a timescale of $\tau \approx 1.1$ hours. It is highly speculative, but that value is similar to the timescale over which we see a decrease in the ≥ 30 keV contributions. Given that whistler-mode waves are known to drive pulsating aurora, could this be one likely explanation? Additional work will be needed to ascertain how relevant this connection is.

The results in Figure 3 are also important in that they confirm the inherent energetic nature of pulsating aurora that previous case studies have suggested. One important reason to study pulsating aurora are the impacts they can have on our atmosphere. Pulsating aurora are very common (Oguti et al., 1981) and can be long-lasting (Jones et al., 2013), thus they could represent an important transfer of energy between the magnetosphere and lower ionosphere. When considering the effects of this transfer, the total energy flux is clearly important, but so too is the contributions from electrons with energies ≥ 30 keV. Higher energy electrons reach further into the atmosphere and thus have a higher probability of influencing terrestrial climate through processes like NO_x based ozone depletion (Turunen et al., 2016; Verronen et al., 2021, & and references therein). We found that the hardest events occur close in time to substorm onset and for high AE indices. In short, our results can be used to more accurately parameterize the atmospheric consequences of pulsating aurora. For instance, combining the results of Figure 3 with those of E. Bland et al. (2021), we can perform a back-of-the-envelope calculation to estimate the incoming power of a typical pulsating aurora event. We will assume an event extending between 62° and 70° magnetic latitude and 4 hours of magnetic local time. Using this, approximately 4.8 gigawatts (GW) of power would be entering the atmosphere during periods with AE > 600 with 2.8 GW coming from ≥ 30 keV electrons. For periods < 20 minutes after substorm onset and all AE indices these values are 2.5 GW and 0.8 GW respectively.

A savvy reader might notice that in Figure 2B it appears that within 20 minutes of substorm onset, what could be considered the expansion phase, is the most common time for our pulsating aurora. That statistic seems to be in contradiction to Partamies et al. (2017), who found that the most common substorm phase for pulsating aurora was the recovery phase. While occurrence rates was not the focus of this work, it is worth examining where this difference could come from. There are two potential reasons. One, our search for pulsating aurora differs. Partamies et al. (2017) only identified pulsating aurora when it was the most dominant type, stating that "...our event selection crite-

ria favors recovery phases over the expansion phases where brighter aurora plays a major role in the auroral displays." Our search included pulsating aurora if we could identify it directly overhead, even when it was not the most visually dominant aurora. Two, Partamies et al. (2017) used a magnetometer at the imager locations while our search was semi local and encompassed a much larger geographic region, so we likely included more substorms in our data set.

Finally, we wanted to point out that other metrics can vary the energy of pulsating aurora besides the ones we looked at. Perhaps most interestingly is the type of pulsating aurora. As Tesema et al. (2020) found, the electron density profile, and thus likely the energy, varies between the types identified by Grono and Donovan (2018). Given the image frequency of our data, we could not accurately distinguish between the different types. However, future studies including pulsating aurora type along with substorm onset and AE index might see an even stronger correlation.

5 Summary

In the field of pulsating aurora, it has been suspected that substorm onset and AE index are linked to variations in the energy flux of the incoming electrons. These suspicions have arisen from studies investigating proxies for energy, such as the altitude of the peak electron density. In this paper, we presented statistical evidence, using inverted energy content, that this hypothesis is correct. When pulsating aurora occurs soon after a substorm onset it is more likely to have a larger total differential energy flux and a harder energy content. This same behaviour also occurs for higher AE indices.

- The differential energy flux of pulsating aurora correlates strongly with the substorm onset and AE index.
- In relation to substorm onset the total differential energy flux varies between 1.15 and 0.63 $\mathrm{mW \cdot m^{-2}}$ for $\leq$ 20 and $>$ 60 minutes. The associated contribution to the total differential energy flux from $\geq$ 30 keV electrons are 33% and 14%.
- In relation to substorms, the differential energy flux remains hard out to 1 hour after onset before softening.
- In relation to AE index the total differential energy flux varies between 2.00 and 0.49 $\mathrm{mW \cdot m^{-2}}$ for $>$ 600 and $\leq$ 200 AE indices. The associated contributions to the total differential energy flux from $\geq$ 30 keV electrons are 59% and 12%.

- We estimate that for a typically pulsating auroral event occurring < 20 min after substorm onset (AE > 600), approximately 2.5 (4.8) GW of power enters the atmosphere. The contributions from ≥ 30 keV electrons are 0.8 (2.8) GW.

Acknowledgments

We acknowledge the help and advice of Robert Marshall, Nithin Sivadas, and Pekka Verronen in developing our inversion analysis.

We acknowledge the substorm timing list identified by the SOPHIE technique (Forsyth et al., 2015), the Newell and Gjerloev technique (Newell & Gjerloev, 2011), the Ohtani and Gjerloev technique (Ohtani & Gjerloev, 2020), the SMU and SML indices (Newell & Gjerloev, 2011); and the SuperMAG collaboration (Gjerloev, 2012).

This material is based upon work supported by the Poker Flat Incoherent Scatter Radar, which is a major facility funded by the National Science Foundation through cooperative agreement AGS-1840962 to SRI International.

RNT was supported by the NASA FINESST award 80NSSC20K1514 to the University of Iowa.

ANJ was supported by NSF CAREER grant 2045016 to the University of Iowa.

SRK was supported by Air Force Office of Scientific Research grant FA9550-19-1-0130 to Clemson University.

References

Bland, E., Tesema, F., & Partamies, N. (2021, February). D-region impact area of energetic electron precipitation during pulsating aurora. *Annales Geophysicae*, *39*(1), 135-149. doi: 10.5194/angeo-39-135-2021

Bland, E. C., Partamies, N., Heino, E., Yukimatu, A. S., & Miyaoka, H. (2019, July). Energetic Electron Precipitation Occurrence Rates Determined Using the Syowa East SuperDARN Radar. *Journal of Geophysical Research (Space Physics)*, *124*(7), 6253-6265. doi: 10.1029/2018JA026437

Davis, T. N. (1978, January). Observed microstructure of auroral forms. *Journal of Geomagnetism and Geoelectricity*, *30*(4), 371-380. doi: 10.5636/jgg.30.371

Dungey, J. W. (1963, June). Loss of Van Allen electrons due to whistlers. *Planetary*

and Space Science, *11*(6), 591-595. doi: 10.1016/0032-0633(63)90166-1

Forsyth, C., Rae, I. J., Coxon, J. C., Freeman, M. P., Jackman, C. M., Gjerloev, J., & Fazakerley, A. N. (2015, December). A new technique for determining Substorm Onsets and Phases from Indices of the Electrojet (SOPHIE). *Journal of Geophysical Research (Space Physics)*, *120*(12), 10,592-10,606. doi: 10.1002/2015JA021343

Gjerloev, J. W. (2012, September). The SuperMAG data processing technique. *Journal of Geophysical Research (Space Physics)*, *117*(A9), A09213. doi: 10.1029/2012JA017683

Gledhill, J. A. (1986, June). The effective recombination coefficient of electrons in the ionosphere between 50 and 150 km. *Radio Science*, *21*(3), 399-408. doi: 10 .1029/RS021i003p00399

Glukhov, V. S., Pasko, V. P., & Inan, U. S. (1992, November). Relaxation of transient lower ionospheric disturbances caused by lightning-whistler-induced electron precipitation bursts. *Journal of Geophysical Research*, *97*(A11), 16971-16979. doi: 10.1029/92JA01596

Grono, E., & Donovan, E. (2018, June). Differentiating diffuse auroras based on phenomenology. *Annales Geophysicae*, *36*(3), 891-898. doi: 10.5194/angeo-36-891 -2018

Hosokawa, K., Miyoshi, Y., Ozaki, M., Oyama, S. I., Ogawa, Y., Kurita, S., ... Fujii, R. (2020, February). Multiple time-scale beats in aurora: precise orchestration via magnetospheric chorus waves. *Scientific Reports*, *10*, 3380. doi: 10.1038/s41598-020-59642-8

Hosokawa, K., & Ogawa, Y. (2015, July). Ionospheric variation during pulsating aurora. *Journal of Geophysical Research (Space Physics)*, *120*(7), 5943-5957. doi: 10.1002/2015JA021401

Jaynes, A. N., Lessard, M. R., Rodriguez, J. V., Donovan, E., Loto'Aniu, T. M., & Rychert, K. (2013, August). Pulsating auroral electron flux modulations in the equatorial magnetosphere. *Journal of Geophysical Research (Space Physics)*, *118*(8), 4884-4894. doi: 10.1002/jgra.50434

Johnstone, A. D. (1978, July). Pulsating aurora. *Nature*, *274*(5667), 119-126. doi: 10.1038/274119a0

Jones, S. L., Lessard, M. R., Fernandes, P. A., Lummerzheim, D., Semeter, J. L.,

Heinselman, C. J., ... Asamura, K. (2009, May). PFISR and ROPA observations of pulsating aurora. *Journal of Atmospheric and Solar-Terrestrial Physics*, *71*(6-7), 708-716. doi: 10.1016/j.jastp.2008.10.004

Jones, S. L., Lessard, M. R., Rychert, K., Spanswick, E., & Donovan, E. (2011, March). Large-scale aspects and temporal evolution of pulsating aurora. *Journal of Geophysical Research (Space Physics)*, *116*(A3), A03214. doi: 10.1029/2010JA015840

Jones, S. L., Lessard, M. R., Rychert, K., Spanswick, E., Donovan, E., & Jaynes, A. N. (2013, June). Persistent, widespread pulsating aurora: A case study. *Journal of Geophysical Research (Space Physics)*, *118*(6), 2998-3006. doi: 10.1002/jgra.50301

Kaeppler, S. R., Sanchez, E., Varney, R. H., Irvin, R. J., Marshall, R. A., Bortnik, J., ... Reyes, P. M. (2020). Chapter 6 - incoherent scatter radar observations of 10–100kev precipitation: review and outlook. In A. N. Jaynes & M. E. Usanova (Eds.), *The dynamic loss of earth's radiation belts* (p. 145-197). Elsevier. Retrieved from `https://www.sciencedirect.com/science/article/pii/B9780128133712000068` doi: https://doi.org/10.1016/B978-0-12-813371-2.00006-8

Kasahara, S., Miyoshi, Y., Yokota, S., Mitani, T., Kasahara, Y., Matsuda, S., ... Shinohara, I. (2018, February). Pulsating aurora from electron scattering by chorus waves. *Nature*, *554*(7692), 337-340. doi: 10.1038/nature25505

Kennel, C. F., & Petschek, H. E. (1966, January). Limit on Stably Trapped Particle Fluxes. *Journal of Geophysical Research (Space Physics)*, *71*, 1. doi: 10.1029/JZ071i001p00001

Lehtinen, N. G., & Inan, U. S. (2007, April). Possible persistent ionization caused by giant blue jets. *Geophysical Review Letters*, *34*(8), L08804. doi: 10.1029/2006GL029051

Lessard, M. R. (2012). A review of pulsating aurora. In *Auroral phenomenology and magnetospheric processes earth and other planets* (Vol. 197, pp. 5673–68). Washington, D.C. :: American Geophysical Union.

Luo, B., Li, X., Temerin, M., & Liu, S. (2013, December). Prediction of the AU, AL, and AE indices using solar wind parameters. *Journal of Geophysical Research (Space Physics)*, *118*(12), 7683-7694. doi: 10.1002/2013JA019188

Marshall, R. A., Xu, W., Kero, A., Kabirzadeh, R., & Sanchez, E. (2019, February). Atmospheric effects of a relativistic electron beam injected from above: chemistry, electrodynamics, and radio scattering. *Frontiers in Astronomy and Space Sciences*, *6*, 6. doi: 10.3389/fspas.2019.00006

Meredith, N. P., Horne, R. B., Johnstone, A. D., & Anderson, R. R. (2000, June). The temporal evolution of electron distributions and associated wave activity following substorm injections in the inner magnetosphere. *Journal of Geophysical Research*, *105*(A6), 12907-12918. doi: 10.1029/2000JA900010

Nanjo, S., Hozumi, Y., Hosokawa, K., Kataoka, R., Miyoshi, Y., Oyama, S.-i., ... Kurita, S. (2021, October). Periodicities and Colors of Pulsating Auroras: DSLR Camera Observations From the International Space Station. *Journal of Geophysical Research (Space Physics)*, *126*(10), e29564. doi: 10.1029/2021JA029564

Newell, P. T., & Gjerloev, J. W. (2011, December). Substorm and magnetosphere characteristic scales inferred from the SuperMAG auroral electrojet indices. *Journal of Geophysical Research (Space Physics)*, *116*(A12), A12232. doi: 10.1029/2011JA016936

Nishimura, Y., Bortnik, J., Li, W., Thorne, R. M., Chen, L., Lyons, L. R., ... Auster, U. (2011, November). Multievent study of the correlation between pulsating aurora and whistler mode chorus emissions. *Journal of Geophysical Research (Space Physics)*, *116*(A11), A11221. doi: 10.1029/2011JA016876

Nishimura, Y., Bortnik, J., Li, W., Thorne, R. M., Lyons, L. R., Angelopoulos, V., ... Auster, U. (2010, October). Identifying the Driver of Pulsating Aurora. *Science*, *330*(6000), 81. doi: 10.1126/science.1193186

Oguti, T., Kokubun, S., Hayashi, K., Tsuruda, K., Machida, S., Kitamura, T., ... Watanabe, T. (1981, August). Statistics of pulsating auroras on the basis of all-sky TV data from five stations. I. Occurrence frequency. *Canadian Journal of Physics*, *59*, 1150-1157. doi: 10.1139/p81-152

Ohtani, S., & Gjerloev, J. W. (2020, September). Is the Substorm Current Wedge an Ensemble of Wedgelets?: Revisit to Midlatitude Positive Bays. *Journal of Geophysical Research (Space Physics)*, *125*(9), e27902. doi: 10.1029/2020JA027902

Oyama, S., Kero, A., Rodger, C. J., Clilverd, M. A., Miyoshi, Y., Partamies, N., ...

Saito, S. (2017, June). Energetic electron precipitation and auroral morphology at the substorm recovery phase. *Journal of Geophysical Research (Space Physics)*, *122*(6), 6508-6527. doi: 10.1002/2016JA023484

Partamies, N., Whiter, D., Kadokura, A., Kauristie, K., Nesse Tyssøy, H., Massetti, S., ... Raita, T. (2017, May). Occurrence and average behavior of pulsating aurora. *Journal of Geophysical Research (Space Physics)*, *122*(5), 5606-5618. doi: 10.1002/2017JA024039

Royrvik, O., & Davis, T. N. (1977, October). Pulsating aurora: Local and global morphology. *Journal of Geophysical Research*, *82*(29), 4720. doi: 10.1029/JA082i029p04720

Sandahl, I., Eliasson, L., & Lundin, R. (1980, May). Rocket observations of precipitating electrons over a pulsating aurora. *Geophysical Research Letters*, *7*(5), 309-312. doi: 10.1029/GL007i005p00309

Semeter, J., & Kamalabadi, F. (2005, April). Determination of primary electron spectra from incoherent scatter radar measurements of the auroral E region. *Radio Science*, *40*(2), RS2006. doi: 10.1029/2004RS003042

Sivadas, N., Semeter, J., Nishimura, Y., & Kero, A. (2017, October). Simultaneous Measurements of Substorm-Related Electron Energization in the Ionosphere and the Plasma Sheet. *Journal of Geophysical Research (Space Physics)*, *122*(10), 10,528-10,547. doi: 10.1002/2017JA023995

Tesema, F., Partamies, N., Nesse Tyssøy, H., & McKay, D. (2020, November). Observations of precipitation energies during different types of pulsating aurora. *Annales Geophysicae*, *38*(6), 1191-1202. doi: 10.5194/angeo-38-1191-2020

Thorne, R. M., Smith, E. J., Fiske, K. J., & Church, S. R. (1974, January). Intensity variation of ELF hiss and chorus during isolated substorms. *Geophysical Research Letters*, *1*(5), 193-196. doi: 10.1029/GL001i005p00193

Tsurutani, B. T., & Smith, E. J. (1974, January). Postmidnight chorus: A substorm phenomenon. *Journal of Geophysical Research (Space Physics)*, *79*(1), 118-127. doi: 10.1029/JA079i001p00118

Turunen, E., Kero, A., Verronen, P. T., Miyoshi, Y., Oyama, S.-I., & Saito, S. (2016, October). Mesospheric ozone destruction by high-energy electron precipitation associated with pulsating aurora. *Journal of Geophysical Research (Atmospheres)*, *121*(19), 11,852-11,861. doi: 10.1002/2016JD025015

Verronen, P. T., Kero, A., Partamies, N., Szelag, M. E., Oyama, S.-I., Miyoshi, Y., & Turunen, E. (2021, October). Simulated seasonal impact on middle atmospheric ozone from high-energy electron precipitation related to pulsating aurorae. *Annales Geophysicae*, *39*(5), 883-897. doi: 10.5194/angeo-39-883-2021

Vickrey, J. F., Vondrak, R. R., & Matthews, S. J. (1982, July). Energy deposition by precipitating particles and Joule dissipation in the auroral ionosphere. *Journal of Geophysical Research*, *87*(A7), 5184-5196. doi: 10.1029/JA087iA07p05184

Whalen, B. A., Miller, J. R., & McDiarmid, I. B. (1971, January). Energetic particle measurements in a pulsating aurora. *Journal of Geophysical Research*, *76*(4), 978. doi: 10.1029/JA076i004p00978

Wing, S., Gkioulidou, M., Johnson, J. R., Newell, P. T., & Wang, C.-P. (2013, March). Auroral particle precipitation characterized by the substorm cycle. *Journal of Geophysical Research (Space Physics)*, *118*(3), 1022-1039. doi: 10.1002/jgra.50160